Extension of the Pierce Model to Multiple Transmission Lines Interacting With an Electron Beam

Venkata Ananth Tamma and Filippo Capolino, *Senior Member, IEEE*

***Abstract*— A possible route toward achieving high-power microwave (HPM) devices is through the use of novel slow-wave structures, represented by multiple coupled transmission lines (MTLs), and whose behavior when coupled to electron beams has not been sufficiently explored. We present the extension of the 1-D linearized Pierce theory to MTLs coupled to a single electron beam. We develop multiple formalisms to calculate the k–ω dispersion relation of the system and find that the existence of a growing wave solution is always guaranteed if the electron propagation constant is larger than or equal to the largest propagation constant of the MTL system. We verify our findings with illustrative examples that bring to light unique properties of the system in which growing waves were found to exist within finite bands of the electron propagation constant and also present possible means to improve the gain. By treating the beam–MTL interaction as distributed dependent current generators in the MTL, we derive relations characterizing the power flux and energy exchange between the beam and the MTLs. For the growing wave, we show that the beam always behaves as an energy source causing power flux along the transmission lines. The theory developed in this paper is the basis for the possible use of degenerate band edges in periodic MTL systems for HPM amplifiers.**

***Index Terms*— Coupled transmission lines, high-power microwaves (HPMs), multiple transmission lines, Pierce model, traveling-wave tubes (TWTs).**

I. Introduction

EVER since their introduction in the 1940s due to the pioneering work of Kompfner, Pierce, and other co-workers, traveling-wave tubes (TWTs) have found immense applications as microwave and millimeter-wave amplifiers in areas, such as RADAR, wireless communications, satellite communications, and electronic counter measure systems, among others. A review of the historical developments and progress achieved in the area of microwave vacuum electronic devices like the TWT is presented in [1]. A simplified and analytical theory of operation of the TWT was described by Pierce as a wave interaction phenomenon [2]–[6]. The 1-D Pierce theory represented the slow-wave structure as an ideal 1-D transmission line (TL) and modeled the electron beam as an 1-D fluid. The amplification produced by the TWT was observed as the result of interaction between the RF signal on the TL with the traveling charge density waves on the electron beam. While the 1-D TL was described by the Telegrapher's equations, the electron beam was described by the equation of continuity and Newton's second law, with both equations expressed in Eulerian coordinates [2], [4], [6]. These inherently nonlinear relations were then linearized under the assumptions of small-signal amplitudes [2], [4]. Due to the linearization, the 1-D Pierce theory fails to account for the saturation of the TWT and does not model the inherent nonlinearities in the TWT. However, despite the apparent oversimplification, the 1-D Pierce model has been used to analytically predict the performance of the TWT in the small-signal regime with reasonable accuracy and has led to the accumulation of substantial physical insights into the operation of TWT-like devices.

In general, a slow-wave structure supports many modes at a given frequency, and therefore the sum of the fields due to these modes would interact with the electron beam. If, however, only one of the modes was to interact with the beam due to the synchronization of their phase velocities, then it would be justified to use the simplified single-TL model as used in Pierce model to analyze the interaction between the beam and the RF fields. However, the exact form of the slow-wave structure does not play a role in the Pierce model due to the very general nature of analysis [6]. Some commonly used slow-wave structures include the helix [6] and its variants, such as the ring-bar and the ring-loop structures [6], and the ladder circuit [7]–[11]. Despite being a popular slow-wave structure due to the inherent simplicity, an important fundamental drawback of the helix is its limited power-handling capacity [6]. Recently, there has been an increased demand for high-power microwave (HPM) devices for both civilian and military applications [12] with the aim of achieving gigawatt peak power levels and very short pulse duration (order of tens of nanoseconds) microwave and millimeter-wave radiation. In light of this demand, it might be beneficial to explore unconventional slow-wave structures with the aim of increasing the peak power levels and the operating efficiency of the TWT. A cursory analysis reveals that the single-TL model does just well enough to reasonably represent the above slow-wave structures at the interaction frequencies thereby justifying its use in the 1-D Pierce model.

Manuscript received May 3, 2013; revised October 23, 2013 and February 3, 2014; accepted February 19, 2014. Date of current version April 8, 2014. This work was supported by AFOSR MURI through the University of New Mexico, Albuquerque, NM, USA, under Grant FA9550-12-1-0489.

The authors are with the Department of Electrical Engineering and Computer Science, University of California, Irvine, CA 92697 USA (e-mail: ananth.tamma@uci.edu; f.capolino@uci.edu).

Color versions of one or more of the figures in this paper are available online at http://ieeexplore.ieee.org.

Digital Object Identifier 10.1109/TPS.2014.2308575

However, the representation of a slow-wave structure as a single TL is one of Pierce theory's major limitations, which can be overcome by the use of multiconductor TLs (MTLs), with each individual TL in the MTL representing a waveguide mode, including mutual coupling among TLs. Typically, slow-wave structures are implemented as periodic circuits, and therefore the operating frequency is chosen to be close to the band edge of the dispersion diagram of the structure.

Previously, MTLs have been applied to TWTs both theoretically and experimentally from a few different perspectives. For example, a distinct TL (helix) was used to efficiently couple the RF signal in and out of the TWT helix at any point without making drastic modifications to the first TWT helix [13], [14]. While the coupled helices were well described using MTLs [13], [14], it should be noted that in [13] and [14] (and references therein), the electron beam was typically assumed to be uncoupled with the external coupling helix (or TL). In addition, Rowe [15] has analyzed multiple interacting electron beam systems theoretically in terms of a coupled MTL system. Furthermore, it was attempted to improve the interaction impedance and gain of a standard helix TWT by the use of multiple helices [16], paralleled TWT circuits and electron beams [17], and multiple ladder circuits [11]. However, the theory developed in [11], [16], and [17] is not general and does not delve into conditions for growing waves and energy conservation.

In the realm of periodic structures, recently, it has been proposed in [18]–[21] that a dramatic increase in field intensity and a vanishing group velocity associated with a degenerate band-edge (DBE) resonance could be achieved by the use of specially arranged periodic arrays of anisotropic layers with misalignment of in-plane anisotropy between the anisotropic layers in a unit cell. Previously, the DBE mode has been observed in periodic stacks of misaligned anisotropic layers [18]–[20], periodically loaded metallic waveguides [22], and coupled waveguiding systems [23], [24]. We anticipate that slow-wave structures exhibiting the DBE mode, modeled by MTLs, if suitably coupled to the electron beam, could be used to design TWTs with unprecedented peak power levels. As an example, we envision the use of DBE structures made up of cascaded hollow metallic waveguide components for applications in HPM devices.

In this paper, we develop a general theory for the interaction of an MTL system with a single electron beam and obtain analytical results for the dispersion diagram of the combined beam–MTL system and derive conditions to obtain growing waves on the coupled MTL–beam system. We also analyze the power flow and energy conservation in the system and derive conditions for power transfer from the beam to the MTL. Section II-F presents illustrative examples for an electron beam coupled to an MTL comprising of multiple identical coupled TLs similar to the examples presented in [11], [16], and [17] and shows an increase in gain similar to the conclusions of [11], [16], and [17]. The theoretical formulation in this paper can be used to analyze MTL systems interacting with a single electron beam, multiple interacting modes in a single waveguide interacting with a single electron beam, and it could be extended to the case of multiple interacting electron beams treated as an MTL system. Finally, but importantly, the presented formulation is the first step toward the analysis MTLs exhibiting a DBE, coupled to an electron beam, which may enable new ways to obtain large gains, and it will be the subject of future investigations.

In particular, here we present an analytical theory analyzing the interaction of an electron beam coupled to a lossless MTL system by extending the Pierce model to the case of MTL and retaining its simplicity. We assume a small-signal approximation and neglect the effect of the space charge forces (those arising from a gradient of the charge density wave) on the longitudinal electric field, as was done in [4] and [6]. Since MTLs can be used to model coupled systems with exotic dispersion characteristics, like for example, DBE modes, the extension of the Pierce model to an MTL system could model the interaction of electron beams with DBE modes in coupled waveguiding systems with applications to HPM devices, to be summarized in future publications. In addition, the Pierce theory with MTLs could be applied to the study of an electron beam interacting with multiple modes in a single real waveguide or to possible novel designs having more than one waveguide interacting with the electron beam.

This paper is organized as follows. In Section II, we develop the theoretical framework for the electron beam and the MTLs and present multiple formalisms to calculate the k–ω dispersion relation including a matrix formulation and a formulation in terms of admittances more akin to the original Pierce derivation. In addition, we discuss the solutions to the dispersion relation with emphasis on identifying the conditions for achieving growing waves and study some illustrative examples. In Section III, we discuss the energy conservation relations for the system and analyze the direction of power flow for plausible solutions of the system.

II. Formulations to Derive k–ω Dispersion Relation

The system of N-TLs coupled among each other by inductive and/or capacitive means and to an electron beam along the $+z$-direction is shown in Fig. 1. The terms s_n and a_n describe how the beam couples to the N-TLs and will be discussed later on in this paper.

A. Electron Beam Dynamics

We follow the linearized equations that describe the space-charge wave on the electron beam presented in [4]. We assume a narrow cylindrical beam of electrons with constant axial electric field across the beam's cross section, and purely longitudinal electron motion and the absence of any transverse electric fields. Let the total electron-wave velocity along $+z$-direction be $u_0 + v$ (m/s), where u_0 is the dc or average value and v is the ac velocity modulation on the beam. We assume a line charge density with units [C/m] given by $\rho_0 + \rho_b$, where ρ_0 is the dc or average value (assumed to be negative) and ρ_b is the ac line charge density modulation on the beam. The total current with units of amperes flowing along the $+z$-direction is $I_0 + I_b$, where I_0 is the dc or average value, and

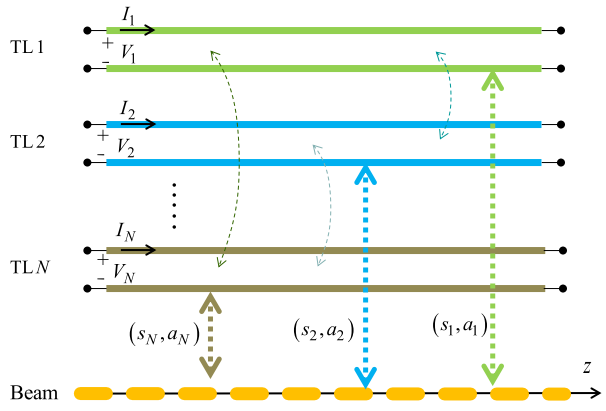

Fig. 1. Schematic diagram describing the N-TLs coupled among each other and to the electron beam.

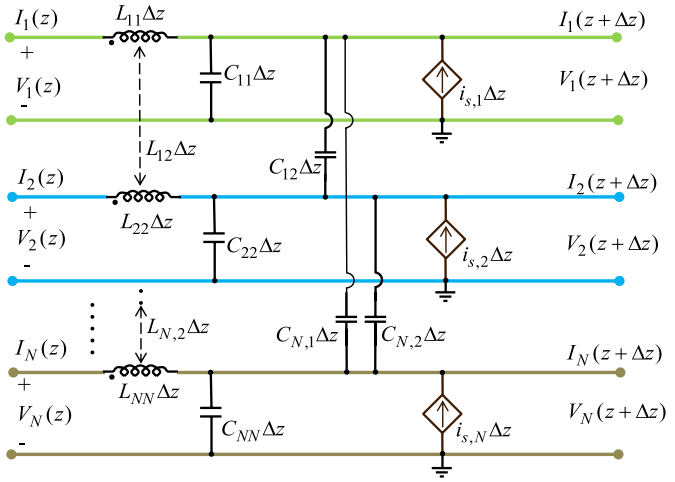

Fig. 2. Schematic diagram showing the current generators per unit length $i_{S,n}$, one each per TL, representing the beam–TL interaction. The TL is schematically shown in terms of its per-unit-length inductances and capacitances along with the coupling inductances and capacitances.

is negative since $I_0 = \rho_0 u_0$, whereas I_b is the ac modulation on the beam.

We denote the charge-to-mass ratio of the electron as $\eta = e/m$, where e is the charge of the electron and is a negative number. The electronic propagation constant is defined as $\beta_0 = \omega/u_0$, where ω is the radian frequency of operation in radian/second. The linearized equations of motion describing the electron beam are written as [4]

$$\partial_t V_b + u_0 \partial_z V_b = u_0 E_z \tag{1}$$

$$I_b = \rho_b u_0 + \rho_0 v. \tag{2}$$

Here, we define an equivalent kinetic beam voltage $V_b = u_0 v/\eta$, with units of volts. We assume that the axial electric field E_z in (1) is the sum of the axial electric fields $E_{z,n}$ of all the N-TL modes

$$E_z = E_{z,1} + E_{z,2} + \cdots + E_{z,N}. \tag{3}$$

It must be noted that the effects of the space charge fields of the electron beam modeled as plasma frequency reduction factor [6] have been neglected in this paper, as was done in [4] and [6]. In addition to (1) and (2), the beam is further described by the 1-D continuity equation $\partial_t(\rho_0 + \rho_b) = -\partial_z(I_0 + I_b)$ that implies $\partial_t \rho_b = -\partial_z I_b$.

B. Formulation of MTL With Current Generators

In the Pierce model, the beam with current $I_0 + I_b$ was assumed to pass very close to the circuit, therefore inducing a current in the TL over the incremental distance Δz [25], [26] and reflected in the TL equations as an equivalent parallel current generator per unit length, with unit (A/m) given by $i_S = -\partial_z I_b$. For N-TLs, we assume that the beam induces a current in every TL such that we consider equivalent parallel current generators on every TL $i_{S,n} = -\partial_z s_n I_b$ or, $\mathbf{i}_S = -\partial_z \mathbf{s} I_b$, and is schematically shown in Fig. 2.

Here, $\mathbf{s} = [s_1, s_2, \ldots, s_N]^T$ is a column vector of dimensionless numbers called current interaction factors. Physically, the components of $\mathbf{s}$ scale the amount of charge induced on the waveguide walls by an electron beam, and hence denote the strength of each shunt current generator induced by the electron beam. In [4] and [5], the current interaction factor was a scalar number with unit value. Here, we include $\mathbf{s}$ to allow for different excitation of distinct TLs. We assume that the charge induced on the waveguide walls by the beam is instantaneous, and hence all elements of $\mathbf{s}$ are assumed to be real numbers. The theoretical formulations for MTLs are well known and the approach presented in [27]–[29] is followed. For the MTL system with parallel current generators, we write the coupled equations as $\partial_z \mathbf{V} = -\underline{\mathbf{L}} \partial_t \mathbf{I}$ and $\partial_z \mathbf{I} = -\underline{\mathbf{C}} \partial_t \mathbf{V} + \mathbf{i}_S$. The TLs are defined by their real distributed (per-unit-length) inductances (L_{lm}) and capacitances (C_{lm}), respectively. If $l = m$, then L_{ll} and C_{ll} represent the self-inductance and self-capacitance of the line l, and if $l \neq m$, then L_{lm} and C_{lm} represent the mutual or coupling inductances and capacitances between lines l and m. We note that the matrices $\underline{\mathbf{L}}$ and $\underline{\mathbf{C}}$ are real symmetric and positive definite [27]–[29]. In addition, $\mathbf{V} = [V_1, V_2, \ldots, V_N]^T$ and $\mathbf{I} = [I_1, I_2, \ldots, I_N]^T$ are the voltages and currents on the TLs. We recall that an MTL system accurately represents wave propagation in a multimode real waveguide.

Considering the voltages and currents on the MTLs to vary with time and distance as $e^{j\omega t} e^{-jkz}$, where k is the complex propagation constant, we rewrite the coupled equations describing MTL in frequency domain as

$$\partial_z \mathbf{V} = -j\omega \underline{\mathbf{L}} \mathbf{I}, \tag{4}$$

$$\partial_z \mathbf{I} = -j\omega \underline{\mathbf{C}} \mathbf{V} + \mathbf{i}_S. \tag{5}$$

Equations (4) and (5) are combined into a single second-order differential equation in $\mathbf{V}$ given by $\left(\partial_z^2 + \omega^2 \underline{\mathbf{L}}\,\underline{\mathbf{C}}\right)\mathbf{V} = -j\omega \underline{\mathbf{L}} \mathbf{i}_S$. Assuming wave solutions, the second-order differential equation is written as

$$\underline{\mathbf{Y}} \mathbf{V} = \mathbf{i}_S \tag{6}$$

where the circuit admittance per unit length [Ω/m] $\underline{\mathbf{Y}}$ is defined as

$$\underline{\mathbf{Y}} = \frac{1}{j\omega} \underline{\mathbf{L}}^{-1} \left(k^2 \underline{\mathbf{1}} - \omega^2 \underline{\mathbf{L}}\,\underline{\mathbf{C}}\right) \tag{7}$$

and $\underline{\mathbf{1}}$ stands for an identity matrix of size $N \times N$. For a single TL, Pierce [4], [5] assumed that the axial electric field

was related to the TL voltage as $E_z = -\partial_z V$. For MTLs, we assume that the axial electric field of the nth TL is related to only the voltage on the nth TL as $E_{z,n} = -a_n \partial_z V_n$ such that the total axial electric field is

$$E_z = -\sum_{n=1}^{N} a_n \partial_z V_n = -\partial_z \left(\mathbf{a}^T \mathbf{V}\right) \tag{8}$$

where $\mathbf{a}^T = [a_1, a_2, \ldots, a_N]$ is a vector of dimensionless real numbers called field interaction factors. Physically, the components of $\mathbf{a}$ describe how much each individual TL affects the electron beam dynamics. In [4] and [5], with a single TL, the field interaction factor was a scalar number with unit value.

C. Derivation of k–ω Dispersion Relation Using Impedance Formulation

We derive a k–ω dispersion relation using an equivalent impedance formulation on the lines of the derivation of the fourth-order equation using impedance concepts in [4] and [5]. It is well known that dependent sources have been used to describe gain in transistors and linear amplifiers, and therefore we find this point of view advantageous even here. The electron beam interaction with the TL system could be completely modeled as an active TL with a voltage-dependent current source, as shown schematically in Fig. 2, given by

$$\mathbf{i}_S = jk\mathbf{s}I_b = -\underline{\mathbf{Y}}_b \mathbf{V} \tag{9}$$

where the electronic beam admittance per unit length [Ω/m] $\underline{\mathbf{Y}}_b$ is defined as

$$\underline{\mathbf{Y}}_b = Y_b \, \mathbf{s}\mathbf{a}^T, \quad Y_b = -j \frac{\eta \rho_0 \beta_0 k^2}{u_0 \left(\beta_0 - k\right)^2} \tag{10}$$

where $\beta_0 = \omega/u_0$. (Note that $Y_b = k^2 Y_e$, where Y_e is the impedance defined in [4] and [5]). We recognize (6) and (9) as the equivalents to the circuit and electronic equations, respectively, in the Pierce theory with for a single TL [1]–[6], [31]. In other words, because of the beam–MTL interaction, the generators can be seen as active admittances, as shown in Fig. 2. The beam admittance per unit length $\underline{\mathbf{Y}}_b$ is derived from the second-order differential equation obtained by combining (1) and (2) and also using (8) for solutions varying with time and distance as $e^{j\omega t} e^{-jkz}$. Equating (6) and (9), the resonance condition for MTLs interacting with an electron beam is

$$\left(\underline{\mathbf{Y}} + \underline{\mathbf{Y}}_b\right) \mathbf{V} = 0 \tag{11}$$

from which we obtain the k–ω dispersion relation by imposing $\mathrm{Det}\left(\underline{\mathbf{Y}} + \underline{\mathbf{Y}}_b\right) = 0$ as

$$\mathrm{Det}\left(\left(k^2 \underline{\mathbf{1}} - \omega^2 \underline{\mathbf{L}}\,\underline{\mathbf{C}}\right) + \frac{\eta \rho_0 \beta_0^2 k^2}{\left(k - \beta_0\right)^2} \underline{\mathbf{L}} \mathbf{s}\mathbf{a}^T \right) = 0. \tag{12}$$

In fact, (12) can be reduced to a polynomial equation of order $(2N + 2)$. This is shown by the use of the fact that for any invertible $(N \times N)$ matrix $\underline{\mathbf{X}}$, any $(N \times 1)$ vector $\mathbf{A}$, and any $(1 \times N)$ vector $\mathbf{B}$, one has $\mathrm{Det}[\underline{\mathbf{X}} + \mathbf{A}\mathbf{B}] = \mathrm{Det}\left[\underline{\mathbf{X}}\right]\left[1 + \mathbf{B}\underline{\mathbf{X}}^{-1}\mathbf{A}\right]$ [30], leading to

$$D(k, \omega)\ P(k, \omega) = 0 \tag{13}$$

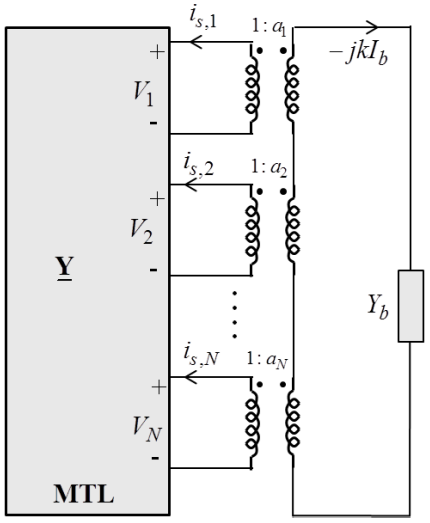

Fig. 3. Schematic diagram showing the transverse resonance condition from a circuit point of view.

where $D(k, \omega) = \mathrm{Det}(k^2 \underline{\mathbf{1}} - \omega^2 \underline{\mathbf{L}}\,\underline{\mathbf{C}})$ and $P(k, \omega) = 1 + k^2 \beta_0^2 \eta \rho_0 \left(k - \beta_0\right)^{-2} \mathbf{a}^T \left(k^2 \underline{\mathbf{1}} - \omega^2 \underline{\mathbf{L}}\,\underline{\mathbf{C}}\right)^{-1} \underline{\mathbf{L}}\mathbf{s}$ are polynomials in k of degree $2N$ and $2N+2$, respectively. The solutions of $D(k, \omega) = 0$ must be disregarded because they imply that $\underline{\mathbf{X}}$ is non invertible. The impedance formulation using dependent current sources can be further explored based on the schematic diagram in Fig. 3, in which the transverse resonance condition is understood from a circuit point of view. We assume that the beam and MTL circuit quantities are interlinked by a transformer as follows. We note that the relation between primary and secondary currents and voltages is $i_{S,n} = s_n \left(jkI_b\right)$ and $-jkI_b = Y_b \sum_{n=1}^{N} a_n V_n$ in Fig. 3, when $s_n = a_n$, i.e., when $\mathbf{s} = \mathbf{a}$, which is what has been traditionally assumed for a single TL interacting with an electron beam [3]–[6]. The circuit also illustrates how each equivalent dependent current generator $i_{S,n}$ depends on the interaction of the beam with the other TLs via the beam impedance per unit length Y_b. It also offers other avenues to find and interpret the resonance condition and power relations in this MTL system. It will be clear that when the beam transfers power to the MTL system, the real part of Y_b is negative, and it is seen to be the only circuit element able to provide power. By inspecting (10), one can observe that power transfer occurs only if k is complex.

D. Derivation of k–ω Dispersion Relation Using a Transfer Matrix Formulation

The first-order differential equations describing the beam and MTLs can be combined into a useful transfer matrix formulation. Assuming wave solutions, (1) is written in frequency domain as $\partial_z V_b = -j\beta_0 V_b + E_z$, and using (8) and (4), we obtain

$$\partial_z V_b = -j\beta_0 V_b + j\omega \mathbf{a}^T \underline{\mathbf{L}}\mathbf{I}. \tag{14}$$

Similarly, (2) is written in frequency domain as $\partial_z I_b = -j\beta_0 I_b + j\omega\eta \left(\rho_0/u_0^2\right) V_b$ and when combined with (5) gives

$$\partial_z \mathbf{I} = -j\omega \underline{\mathbf{C}}\mathbf{V} + j\beta_0 \mathbf{s} I_b - j\omega\eta \frac{\rho_0}{u_0^2} \mathbf{s} V_b. \tag{15}$$

Collecting the frequency-domain forms of (1) and (2) along with (14) and (15), the coupled beam–MTL system could be represented by the set of $(2N+2)$ first-order equations written in condensed matrix form

$$\partial_z \boldsymbol{\psi}(z) = -j\underline{\mathbf{M}}\,\boldsymbol{\psi}(z) \tag{16}$$

where we define the state vector $\boldsymbol{\psi}(z) = \left[\mathbf{V}\ \mathbf{I}\ V_b\ I_b\right]^T$. The matrix $\underline{\mathbf{M}}$ of size $(2N+2)\times(2N+2)$ is

$$\underline{\mathbf{M}} = \begin{bmatrix} \mathbf{0} & \omega\underline{\mathbf{L}} & \mathbf{0} & \mathbf{0} \\ \omega\underline{\mathbf{C}} & \mathbf{0} & \omega\eta\frac{\rho_0}{u_0^2}\mathbf{s} & -\beta_0\mathbf{s} \\ \mathbf{0} & -\omega\left(\mathbf{a}^T\underline{\mathbf{L}}\right) & \beta_0 & 0 \\ \mathbf{0} & \mathbf{0} & -\omega\eta\frac{\rho_0}{u_0^2} & \beta_0 \end{bmatrix}. \tag{17}$$

We recognize (16) to be the well-known Cauchy problem and assuming known initial conditions $\boldsymbol{\psi}(z_0) = \boldsymbol{\psi}_0$, the solution of (16) is written as $\boldsymbol{\psi}(z_1) = \underline{\mathbf{T}}(z_1, z_0)\,\boldsymbol{\psi}(z_0)$, where we define $\underline{\mathbf{T}}(z, z_0)$ as the transfer matrix that uniquely relates the state vector $\boldsymbol{\psi}(z)$ between two known points z_0 and z_1 along the z-axis. The transfer matrix formulation is also useful to analyze periodic systems, such as coupled TLs, exhibiting a DBE condition and will be elaborated in future publications. The propagation constants of the coupled system could be obtained directly by calculating the eigenvalues of the matrix $\underline{\mathbf{M}}$, or the k-ω dispersion relation of the coupled system could be obtained directly by evaluating the characteristic equation $\mathrm{Det}\left(\underline{\mathbf{M}} - k\underline{\mathbf{1}}\right) = 0$ of the matrix $\underline{\mathbf{M}}$. For N-TLs, the number of roots of the characteristic equation and hence the number of propagation constants of the system is $(2N+2)$. Following the derivation in Appendix A, $\mathrm{Det}\left(\underline{\mathbf{M}} - k\underline{\mathbf{1}}\right) = 0$ can be reduced to the form given in (13), which leads to a polynomial equation of degree $2N+2$ in k, and thus yielding $2N+2$ roots. We note that both this formulation and the one in Section II-C yield the same k–ω dispersion relation. A form of (13) with $\underline{\mathbf{L}}, \underline{\mathbf{C}}$ matrices in diagonal form is presented in Appendix B.

E. Solutions of the k–ω Dispersion Relation

Since the dispersion relation in (13) is a product of two functions, for any fixed ω, the solutions of (13) contain the solutions obtained from the conditions $D(k,\omega) = 0$ and $P(k,\omega) = 0$. The condition $D(k,\omega) = 0$, yields the $2N$ natural propagation constants $\{\beta_{c,1}, \beta_{c,2}, \ldots, \beta_{c,N}\}$ of the MTL uncoupled to the electron beam. However, it is evident from (13) that the solutions of $D(k,\omega) = 0$ cannot be solutions of $P(k,\omega) = 0$ and must be disregarded. Following the brief proof presented in Appendix B, for the N-line system coupled to electron beam, the existence of a complex conjugate root, and hence the existence of increasing and decreasing waves, is always guaranteed if

$$\beta_0 \geq \max\left\{\beta_{c,1}, \beta_{c,2}, \ldots, \beta_{c,N}\right\}. \tag{18}$$

A more general mathematical proof of (18) can be found in [32] stating that there are at most two complex roots, and that these are always found if (18) is satisfied. Due to (18), we can obtain $2N$ purely real propagation constants $k = (\beta_1, \beta_2, \beta_3, \ldots, \beta_{2N})$ and complex conjugate solutions $k = \beta \pm j\alpha$. We numerically explore (18) for some illustrative examples in Section II-F. From Figs. 5–8, a complex k solution is always found for β_0 satisfying (18). Furthermore, in the range $\min\{\beta_{c,n}\} < \beta_0 < \max\{\beta_{c,n}\}$, complex conjugate roots are seen to exist only when β_0 is in the vicinity of $\beta_{c,n}$. We find then a resonant-like behavior in $\mathrm{Im}(k)$ when $\beta_0 \to \beta_{c,n}$ in which $\mathrm{Im}(k)$ is seen to peak when $\beta_0 \approx \beta_{c,n}$ and then decays for β_0 larger than $\beta_{c,n}$, eventually approaching zero. In general, complex roots could also be found when $\beta_0 < \min\{\beta_{c,n}\}$ under certain conditions, as shown in [32], where a graphical analysis to determine the roots is also provided.

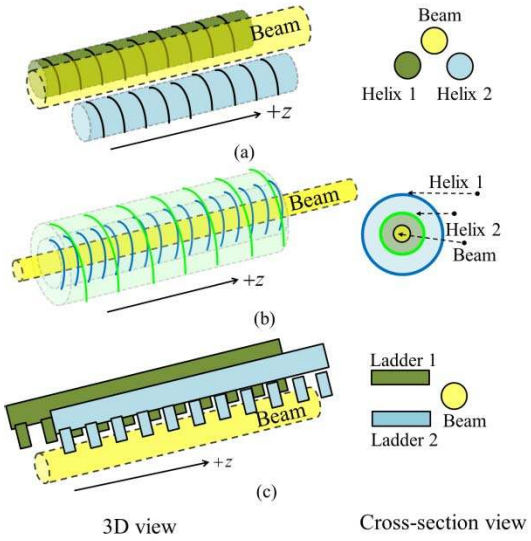

Fig. 4. Illustrative schematics showing the two coupled slow-wave structures interacting with a single electron beam. The structures are (a) multiple helices placed next to each other, (b) multiple coaxial helices, and (c) multiple ladder circuits. Also shown next to each schematic view is the cross-sectional view of the structure for better understanding.

F. Illustrative Examples Showing Condition for Growing Waves

Inequality (18) establishing the condition for growing waves is numerically investigated for $N = 2$ TL-beam systems for various parameters. The parameters used in the numerical studies are detailed in Appendix C. The propagation constants were obtained by evaluating the eigenvalues of (17). An idealized physical picture of the $N = 2$ TL-beam system can be viewed as the interaction between two coupled slow-wave structures modeled as an MTL and a single electron beam shown in Fig. 4, which details three different possible physically realizable interaction configurations and geometries. Fig. 4(a) shows two electromagnetically coupled helices, each interacting with a single electron beam and placed close to each other (in a side-by-side configuration) with the beam propagating close to the surface of the helices and also in the gap between the helices. Fig. 4(b) shows another configuration using two electromagnetically coupled helices with both the helices and the beam to be coaxial with each other [13], [14]. The configuration in Fig. 4(c) is similar to that of Fig. 4(a) in that the two electromagnetically coupled ladder circuits [11], each interacting with a single electron beam, are placed close to each other (in a side-by-side configuration) with

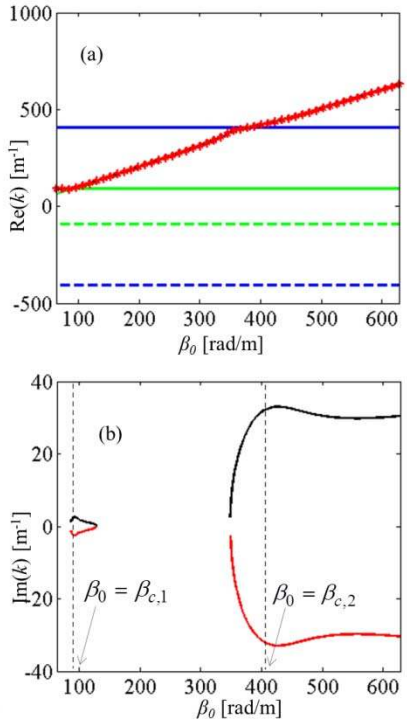

Fig. 5. Plots of (a) real values (β) of the six k solutions are plotted of which four correspond to two forward ($\beta > 0$) and two backward ($\beta < 0$) waves with purely real constant values equal to $+\beta_1, +\beta_2$ and $-\beta_1, -\beta_2$, respectively, while remaining two correspond to real part of the complex growing wave solutions and (b) imaginary parts of the six solutions for k for a two-TL system coupled to the electron beam versus β_0.

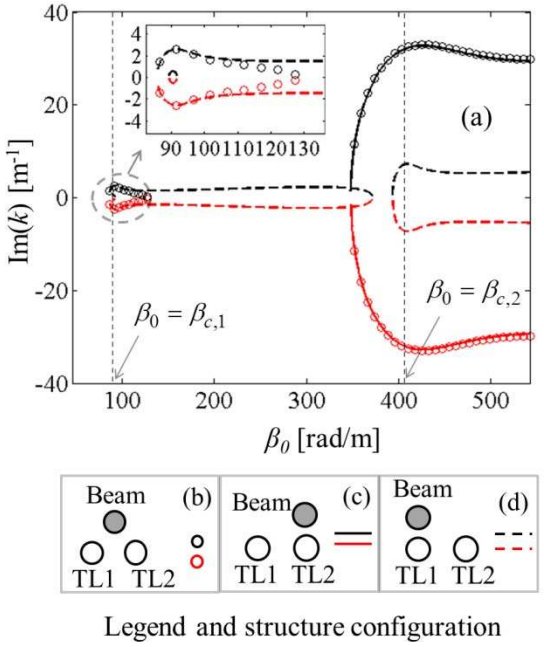

Fig. 6. Plots of (a) imaginary parts of k for a two-TL system coupled to the electron beam versus β_0 with the different configurations of coupling shown in (b)–(d). Inset in (a) shows a zoomed-in region at $\beta_0 \rightarrow \beta_{c,1}$.

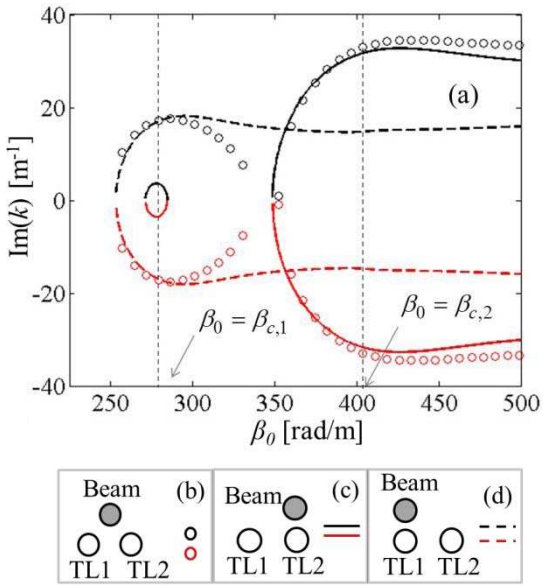

Fig. 7. Plots of (a) imaginary parts of k for a two-TL system coupled to the electron beam versus β_0 with the different configurations of coupling shown in (b)–(d). The two TLs have different characteristic impedances. The configurations in (b)–(d) are identical to those in Fig. 6(b)–(d).

the beam grazing the surfaces of both the ladder circuits while propagating in the gap between both the ladders. The cross-sectional views corresponding to each of the structural arrangements in Fig. 4(a)–(c) are shown next to each of the respective 3-D views. We assume that the electromagnetic interaction between the coupled slow-wave structures can be varied either by structural modifications or by increasing the spatial separation between them. We also assume that the values of **s** and **a**, which signify the interaction of the structure with the beam, can be varied by moving the spatial position of the beam with respect to the structures. For simplicity, we choose to analyze the configuration of Fig. 4(a) in the subsequent numerical examples within the constraints of the TL approximation. In particular, we model the electromagnetic interactions between the two coupled helices as coupling inductance and capacitance.

As an illustrative example, we first consider two TLs with different values of equivalent line inductances and capacitances interacting equally with the electron beam with $\mathbf{s} = \mathbf{a} = \mathbf{1}$, where **1** defines a column vector of ones. The real (β) and imaginary parts (α) of the six solutions for the propagation constant k of the mode supported by the two-TL system are plotted in Fig. 5 versus β_0 obtained by keeping ω constant and varying the dc electron velocity u_0. In Fig. 5, the six k solutions are plotted: two are complex valued and four are real. In particular, of the four real valued solution, two are forward ($\beta > 0$) and two are backward ($\beta < 0$) waves, denoted as $+\beta_1, +\beta_2$ and $-\beta_1, -\beta_2$, respectively. The remaining two complex solutions have identical real values of k in Fig. 5(a), seen to linearly increase with β_0, and correspond to the complex conjugate roots $\beta \pm j\alpha$, whose imaginary parts are plotted in Fig. 5(b). Inequality (18) is confirmed in Fig. 5(b), which shows that the Im(k) is nonzero for $\beta_0 \geq \max\{\beta_{c,1}, \beta_{c,2}\}$, where we assume $\beta_{c,2} > \beta_{c,1}$. In addition, we observe that Im(k) is nonzero in the vicinity of $\beta_0 = \beta_{c,1}$. However, it is seen that the Im(k) vanishes for a large range of β_0 when $\beta_{c,1} < \beta_0 < \beta_{c,2}$.

It is seen that the plot of Im(k) versus β_0 is a continuous curve and different than zero when $\beta_0 \geq \beta_{c,2}$, whereas in the range $\beta_{c,1} \leq \beta_0 < \beta_{c,2}$, it is seen that Im($k$) is nonzero only within certain discrete bands that occur when $\beta_0 \to \beta_{c,n}$. Further numerical investigation with $N \geq 3$ confirmed this trend, and in general, it is found that Im(k) has a continuous spectrum different than zero when $\beta_0 \geq \max(\beta_{c,1}, \beta_{c,2}, \ldots, \beta_{c,N})$ and in the range of $\min\{\beta_{c,n}\} < \beta_0 < \max\{\beta_{c,n}\}$, where $1 \leq n \leq N$, it is seen that Im(k) is nonzero only within certain discrete bands that occur when $\beta_0 \to \beta_{c,n}$.

While the spectrum of Im(k) plotted in Fig. 5(b) was computed for equal interaction of the two TLs with different values of equivalent line inductances and capacitances with a single electron beam, in Fig. 6, we plot the spectrum of the same two TLs but interacting unequally with the electron beam, i.e., different values of **s** and **a**, given in Appendix C. In particular, the physical picture of the interaction corresponds to the various positions of the beam with respect to the two TLs, as shown in Fig. 6(b)–(d), which details the way the beam interacts with each of the TLs. When the beam is closer to only one of the TLs like in Fig. 6(c) and (d), we assume that the TL closest to the beam interacts strongly with the beam and hence has a larger values of s_n and a_n, while the other TL located farther away from the beam interacts weakly with the beam and has lower values of s_n and a_n. The influence of varying **s** and **a** of the MTL system is seen in the plots of Im(k) in Fig. 6(a) for each of the physical situation shown in Fig. 6(b)–(d). In particular, for the physical situation in Fig. 6(b), both the TLs interact equally, i.e., same values of s_n and a_n, with the electron beam and the results are same as those plotted in Fig. 5(b). Note that the values of Im(k) when $\beta_0 \to \beta_{c,1}$ are much smaller than the values of Im(k) when $\beta_0 \geq \beta_{c,2}$. This is in contrast with the plot of Im(k) corresponding to the physical situation shown in Fig. 6(d), in which TL1 is closer to the beam than TL2 and hence $s_1 = a_1 > s_2 = a_2$ diminishing the values of Im(k) when $\beta_0 \geq \beta_{c,2}$. The inset of Fig. 6(a) shows a zoomed-in plot of Im(k) close to the discrete band occurring when $\beta_0 \to \beta_{c,1}$. The influence of **s** and **a** can be further seen in the plot of Im(k) corresponding to the physical situation shown in Fig. 6(c), in which TL2 is closer to the beam than TL1 and hence $s_1 = a_1 < s_2 = a_2$. For this case, the values of Im(k) when $\beta_0 \to \beta_{c,1}$ are negligible when compared with the values of Im(k) for $\beta_0 \geq \beta_{c,2}$ as clearly shown in the inset of Fig. 6(a). From the numerical values used to compute the results plotted in Fig. 6, which are detailed in Appendix C, we note that the electromagnetic coupling between the two TLs is chosen to be small but the results plotted in Fig. 6(a) are also valid for stronger coupling.

For the case of zero electromagnetic coupling between the two TLs, the characteristic impedance (and hence the interaction impedance [5]) of TL2 is about 4.5 times larger than that of TL1. In addition to the different values of **s** and **a**, the effect of different values of the characteristic impedance of the TLs on Im(k) was further investigated and the result of one such investigation is plotted in Fig. 7 while maintaining the same physical configurations as in Fig. 6(b)–(d). The electromagnetic coupling between the two TLs is chosen

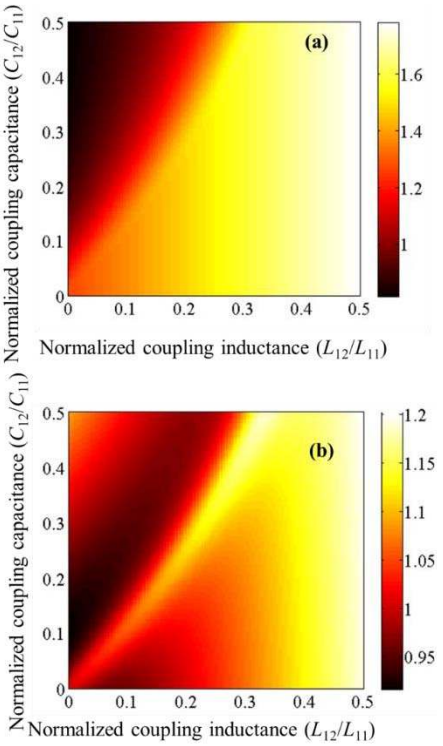

Fig. 8. Plot of ratio of Im(k) of two-TL system to Im(k) of one-TL system [Im $(k)_{2-\mathrm{TL}}$ /Im $(k)_{1-TL}$] versus the variations in the normalized coupling inductance and capacitance between the two TLs. The two TLs are coupled to an electron beam with (a) equal and (b) unequal beam–TL interaction.

to be small and such that for the case of vanishing coupling, the characteristic impedance of TL2 is just $\sqrt{2}$ times larger than that of TL1. Again, the plot in Fig. 7(a) shows the same trends for Im(k) as that plotted in Fig. 6(a) for the three distinct physical interaction configurations in Fig. 7(b)–(d), which are identical to those in Fig. 6(b)–(d). However, we note that the change in ratio of characteristic impedance affects the values of Im(k) (in both the regions when $\beta_0 \to \beta_{c,1}$ and when $\beta_0 \geq \beta_{c,2}$) for the different **s** and **a** values corresponding to the various physical configurations shown in Fig. 7(b)–(d).

The results plotted in Figs. 6 and 7 clearly show that the choice of beam–TL coupling and characteristic impedance of the TL significantly affect Im(k) of the combined system. Careful consideration needs to be given to various structural and beam coupling parameters during the design of any MTL–beam system.

The dependence on structural and coupling parameters is further investigated in Fig. 8(a) and (b), which show the effect on Im(k) of the variation of the coupling inductances and capacitances of a two-TL system with identical lines, coupled among themselves and to a single electron beam. Here, we plot the ratio of Im(k) of the two-TL system to the Im(k) of an one-TL system [Im $(k)_{2-\mathrm{TL}}$ /Im $(k)_{1-TL}$] as a function of the variation in the normalized coupling inductance (L_{12}/L_{11}) and normalized coupling capacitance (C_{12}/C_{11}) of the two-TL system with identical lines. Here, L_{12} and C_{12} are the coupling inductance and capacitance, between the two TLs. In addition, L_{11} and C_{11} denote the self-inductance and capacitance, of both the identical TLs (i.e., $L_{11} = L_{22}$ and $C_{11} = C_{22}$).

A wide range of values of coupling inductance and capacitance were considered so as to include cases of both weak and strong coupling. In Fig. 8, we vary L_{12} and C_{12} from zero (i.e., no coupling between TLs) to half the value of L_{11} and C_{11}, respectively (strong coupling between TLs). The Im(k) of the one-TL system was calculated by considering L_{11} and C_{11} as the self-inductance and (-)capacitance, respectively. The plot in Fig. 8(a) corresponds to physical picture of TL–beam interaction shown in Fig. 6(b) [or Fig. 7(b)] indicating equal beam–TL interaction, whereas the plot in Fig. 8(b) corresponds to physical picture of interaction shown in Fig. 6(d) [or Fig. 7(d)] indicating unequal beam–TL interaction. The numerical values of **s** and **a** used in the computations are detailed in Appendix C.

The results in Fig. 8 clearly identify ranges of normalized coupling inductance and capacitance in which the Im(k) of the two-TL system can be either larger or smaller than the Im(k) of the one-TL system, and for different beam–TL interactions. Once again, this suggests that for suitable structural and beam–TL coupling parameters, a two-TL system (coupled to an electron beam) could have larger values of Im(k) than an one-TL system coupled to an electron beam. For all calculations related to the two-TL system, we have assumed $\beta_0 = \max\{\beta_{c,1}, \beta_{c,2}\}$ to always ensure the existence of growing waves in the TL–beam system. In addition, note that when $L_{12} = 0$ H/m and $C_{12} = 0$ F/m [corresponding to the origin in Fig. 8(a) and (b)], we know that $\beta_0 = \beta_{c,1} = \beta_{c,2} = \beta_c$, where we denote as β_c the propagation constant of the one-TL system; in this case, we obtain $\mathrm{Im}\,(k)_{2-\mathrm{TL}} = 1.26\ \mathrm{Im}\,(k)_{1-TL}$ in Fig. 8(a) and $\mathrm{Im}\,(k)_{2-\mathrm{TL}} = \mathrm{Im}\,(k)_{1-TL}$ in Fig. 8(b). This shows that two identical TLs uncoupled to each other can have $\mathrm{Im}\,(k)$ larger than $\mathrm{Im}\,(k)_{1-TL}$ with same line parameters for certain beam–TL coupling conditions. However, we do note that the two uncoupled TLs are still coupled to each other through the electron beam, as discussed in Section II-C and Fig. 3. Furthermore, a proper choice of TL coupling parameters can further increase the value of $\mathrm{Im}\,(k)$ compared with $\mathrm{Im}\,(k)_{1-TL}$. While the importance of interaction impedance and the values of **s** and **a** are clearly highlighted in the results plotted in Figs. 6–8, it is clear from Fig. 8(a) and (b) that $\mathrm{Im}\,(k)_{2-\mathrm{TL}} > \mathrm{Im}\,(k)_{1-TL}$ for only certain parameter ranges. We envision that by introducing periodic MTL systems operating near the Brillouin zone edge, the stored electromagnetic energy density in the MTL could be much higher than the corresponding density in the one-TL system.

III. Power Flow Analysis

Since the beam was included in the active MTL model as voltage-dependent current sources, the power transfer from the beam to the TLs would be equivalent to the power supplied by the dependent current sources to the MTL, which is analyzed next.

A. Energy Conservation

To show the energy conservation in the active TL system, we define for the N-line system, the flux of complex power along the nth TL as $S_{f,n} = (1/2)V_n I_n^*$, and denote the time-average power flux as $P_{f,n} = \mathrm{Re}(S_{f,n})$. Therefore, the total complex power flux in the N-TLs at any z is

$$S_f = \sum_{n=1}^{N} S_{f,n} = \frac{1}{2}\mathbf{V}^T\mathbf{I}^*. \tag{19}$$

Consider the variation of complex power along the MTL, $\partial_z S_f = (1/2)\left(\partial_z \mathbf{V}^T\right)\mathbf{I}^* + (1/2)\mathbf{V}^T\left(\partial_z \mathbf{I}^*\right)$. Using the transpose and complex conjugates of (4) and (5), we obtain $\partial_z S_f + (1/2)j\omega\left(\mathbf{I}^T\underline{\mathbf{L}}\mathbf{I}^* - \mathbf{V}^T\underline{\mathbf{C}}\mathbf{V}^*\right) = S_S$, which is interpreted as an 1-D Poynting theorem with the term $S_S = (1/2)\mathbf{V}^T\mathbf{i}_S^*$ representing the total complex power delivered per unit length by all the dependent current sources. The term $\partial_z S_f$ is seen as the power flux in the TL along the $+z$-direction, whereas the term $j\omega(1/2)\left(\mathbf{I}^T\underline{\mathbf{L}}\mathbf{I}^* - \mathbf{V}^T\underline{\mathbf{C}}\mathbf{V}^*\right)$ is purely imaginary, with $(1/2)\mathbf{I}^T\underline{\mathbf{L}}\mathbf{I}^*$ and $(1/2)\mathbf{V}^T\underline{\mathbf{C}}\mathbf{V}^*$ the stored magnetic and electric energy line densities, respectively.

B. Evaluation of Time-Average Power Delivered by Dependent Current Sources

For the N-line system, the time-average power delivered by each dependent current source $i_{S,n}$ is $P_{S,n} = (1/2)\mathrm{Re}(V_n i_{S,n}^*)$, and therefore the total time-average power delivered by the N dependent current generators is $P_S = \sum_{n=1}^{N} P_{S,n} = \mathrm{Re}\,(S_S)$. Using (6), we express P_S in terms of the circuit admittance $\underline{\mathbf{Y}}$ as

$$P_S = \tfrac{1}{2}\mathrm{Re}\left(\mathbf{V}^T\underline{\mathbf{Y}}^*\mathbf{V}^*\right) = \tfrac{1}{2}\mathrm{Re}\left(-\frac{(k^*)^2}{j\omega}\mathbf{V}^T\underline{\mathbf{L}}^{-1}\mathbf{V}^*\right) \tag{20}$$

where we dropped the term $j\omega\mathbf{V}^T\underline{\mathbf{C}}\mathbf{V}^*$ as it is always purely imaginary for any real ω, and hence does not contribute to the time-average power delivered to the TLs. Since $\underline{\mathbf{L}}$ and therefore $\underline{\mathbf{L}}^{-1}$ is a real symmetric positive-definite matrix, the quadratic form $F(z) = \mathbf{V}^T\underline{\mathbf{L}}^{-1}\mathbf{V}^* = \sum_{n=1}^{N}\lambda_{L,n}^{-1}|\mathbf{t}_{I,n}^T\mathbf{V}|^2 > 0$, where $\mathbf{t}_{I,n}$ are the eigenvectors of $\underline{\mathbf{L}}^{-1}$ associated with the eigenvalue $\lambda_{L,n}^{-1}$, and $\lambda_{L,n}$ are the eigenvalues of the matrix $\underline{\mathbf{L}}$. It is convenient to express the voltages in terms of their initial condition as $V_n = V_{n0}e^{j\omega t}e^{-j\beta z}e^{\pm\alpha z}$ such that $|\mathbf{t}_{I,n}^T\mathbf{V}|^2 = |\mathbf{t}_{I,n}^T\mathbf{V}_0|^2 e^{\pm 2\alpha z}$ for two conjugate roots $k = \beta \pm j\alpha$, and define $F_0 = \sum_{n=1}^{N}\lambda_{L,n}^{-1}|\mathbf{t}_{I,n}^T\mathbf{V}_0|^2 > 0$. Then, the time-average power delivered by the dependent current sources in terms of the circuit admittance $\underline{\mathbf{Y}}$ is

$$P_S = \pm\frac{\alpha\beta}{\omega}e^{\pm 2\alpha z}F_0 \tag{21}$$

where we have used the relation $\mathrm{Re}[j(k^*)^2] = \pm 2\alpha\beta$. The power delivered to the TL is different from zero for complex $k = \beta \pm j\alpha$. Using (11), the time-average power delivered by the dependent current sources can also be written in terms of the beam admittance $\underline{\mathbf{Y}}_b$ as $P_S = -(1/2)\mathrm{Re}(\mathbf{V}^T\underline{\mathbf{Y}}_b^*\mathbf{V}^*) = -(1/2)\mathrm{Re}[Y_b^*(\mathbf{V}^{*^T}\mathbf{s}\mathbf{a}^T\mathbf{V})^*]$. We identify $\mathbf{V}^{*^T}\mathbf{s}\mathbf{a}^T\mathbf{V}$ as the quadratic form and observe that $\mathbf{s}\mathbf{a}^T$ has only one nonzero eigenvalue $\lambda_1 = \sum_{n=1}^{N}(s_n a_n)$ and has $N-1$ vanishing eigenvalues. The eigenvalue λ_1 is real since we assumed that both **s** and **a** are composed of real

numbers. Therefore, the time-average delivered power in terms of the beam admittance $\underline{\mathbf{Y}}_b$ is

$$P_S = -\frac{1}{2}\frac{\eta\beta_0\rho_0}{u_0}\lambda_1\left|\mathbf{q}'^T_1\mathbf{V}\right|^2\mathrm{Re}\left[\frac{j\,(k^*)^2}{(\beta_0-k^*)^2}\right] \tag{22}$$

where $\mathbf{q}'_1$ is the eigenvector of $\mathbf{s}\mathbf{a}^T$ associated with the eigenvalue λ_1. This also shows that time average power is delivered by the electron beam when k is complex, as it will be shown later in more details.

C. Summary on Power Transfers for Real and Complex Conjugates k

The power transferred from the beam to the $N-$coupled TL system is given by (21), which, however, depends on the complex value of the propagation constant k. From Section II-E, if (18) is satisfied, we find that k has $2N$ real roots, $k = (\beta_1, \beta_2, \beta_3, \ldots, \beta_{2N})$, and two conjugate roots $k = \beta \pm j\alpha$. We want to clarify the value and direction of power transferred under these conditions.

Let us consider first the case of the mth real root $k = \beta_m$. Since $\mathbf{V}^T\underline{\mathbf{L}}^{-1}\mathbf{V}^*$ in (20) is purely real and positive, we find P_S to be purely imaginary. Therefore, we have no power transferred between the electron beam and the MTL, i.e., $P_S = 0$. Next, we investigate the value and direction of time-averaged power transferred for the complex root $k = \beta \pm j\alpha$. In this case, we consider the time-average power delivered to the MTL by all the sources per unit length given in (21). Therefore, from (21), if we assume $\beta > 0$, the real power is always transferred from the electron beam to the MTLs in the case of $\alpha > 0$, and vice versa, the power is transferred from the MTL to the beam when $\alpha < 0$.

D. Power Flux Along the MTL

For the MTL system, the total complex power flux in the N-TL system at any z is given by (19) and the time-averaged flux is given by $P_f = \mathrm{Re}\left(S_f\right)$. Using (4)–(6) in (19), we obtain

$$P_f = \tfrac{1}{2}\mathrm{Re}\big(\tfrac{k^*}{\omega}\mathbf{V}^T\underline{\mathbf{L}}^{-1}\mathbf{V}^*\big) = \tfrac{1}{2}\mathrm{Re}\left(\tfrac{k}{\omega}\right)e^{\pm 2\alpha z}F_0 \tag{23}$$

which shows that there is always a *positive flux* of power in the MTL along the $+z$-direction for $\mathrm{Re}\,(k) > 0$. If we take the ratio of P_S/P_f for the complex conjugate wavenumber $k = \beta \pm j\alpha$, we obtain

$$\frac{P_S}{P_f} = \pm 2\alpha. \tag{24}$$

This means that the ratio of power transferred from the electron beam to the entire MTL system, over the power carried in the MTL system, depends only on the value of $\pm\alpha$.

E. Analysis of Complex Power Transfer

From (7) and (10), it is observed that the circuit and beam admittances depend on the complex propagation constant $k = \beta \pm j\alpha$, and therefore are decomposed into real and imaginary components. Accordingly, for $k = \beta + j\alpha$, $\underline{\mathbf{Y}} = \underline{\mathbf{Y}}_r + j\underline{\mathbf{Y}}_i$ and $\underline{\mathbf{Y}}_b = \underline{\mathbf{Y}}_{b,r} + j\underline{\mathbf{Y}}_{b,i}$. When higher powers of α were neglected assuming $|\alpha| << |\beta|$, the real and imaginary parts can be simplified as $\underline{\mathbf{Y}}_r = (2\beta\alpha/\omega)\underline{\mathbf{L}}^{-1}$, $\underline{\mathbf{Y}}_i \cong -(\underline{\mathbf{L}}^{-1}/\omega)[\beta^2\underline{\mathbf{1}} - \omega^2\underline{\mathbf{L}}\,\underline{\mathbf{C}}]$, and $\underline{\mathbf{Y}}_{b,r} \cong 2\beta_0\beta\alpha(\beta_0-\beta)G_0\mathbf{s}\mathbf{a}^T$, $\underline{\mathbf{Y}}_{b,i} \cong -(\beta^2(\beta_0-\beta)^2 - 3\alpha^2\beta_0^2 + 2\alpha^2\beta\beta_0)G_0\mathbf{s}\mathbf{a}^T$ with $G_0 = (\beta_0\eta\rho_0/u_0)/[(\beta_0-\beta)^2+\alpha^2]^2 > 0$.

The resonance condition (11) implies that $\underline{\mathbf{Y}}$, $\underline{\mathbf{Y}}_b$ and the complex power are related by the quadratic form $\mathbf{V}^T\underline{\mathbf{Y}}^*\mathbf{V}^* + \mathbf{V}^T\underline{\mathbf{Y}}_b^*\mathbf{V}^* = 0$. This identity must be simultaneously verified for real and imaginary power terms, leading to $\mathbf{V}^T\underline{\mathbf{Y}}_r^*\mathbf{V}^* + \mathbf{V}^T\underline{\mathbf{Y}}_{b,r}^*\mathbf{V}^* = 0$ and $\mathbf{V}^T\underline{\mathbf{Y}}_i^*\mathbf{V}^* + \mathbf{V}^T\underline{\mathbf{Y}}_{b,i}^*\mathbf{V}^* = 0$.

First, considering the real power terms, we can expand $\mathbf{V}^T\underline{\mathbf{Y}}_r^*\mathbf{V}^* + \mathbf{V}^T\underline{\mathbf{Y}}_{b,r}^*\mathbf{V}^* = 0$ as

$$\frac{1}{\omega}F + \beta_0\,(\beta_0-\beta)\,G_0\lambda_1\left|\mathbf{q}'^T_1\mathbf{V}\right|^2 = 0. \tag{25}$$

The first term in (25) is the contribution from $\underline{\mathbf{Y}}_r$ and is positive, while the second term is from $\underline{\mathbf{Y}}_{b,r}$, which may assume both signs depending on $(\beta_0-\beta)$. Therefore, (25) could be satisfied for some ω only if $\beta > \beta_0$ and $\lambda_1 > 0$ (note that $\lambda_1 > 0$ is also true if $\mathbf{s} = \mathbf{a}$), because under this condition, the terms in (25) always have opposite signs. In summary, if $\beta > \beta_0$ and $\alpha > 0$, then $2\beta_0\beta\alpha\,(\beta_0-\beta) < 0$, and thereby the real power $P_S = (-1/2)\mathrm{Re}(\mathbf{V}^T\underline{\mathbf{Y}}_{b,r}^*\mathbf{V}^*)$ associated to $\underline{\mathbf{Y}}_{b,r}$ is always positive causing power flow from the beam to the MTL when (11) holds true. Vice versa if $\beta < \beta_0$ and $\alpha > 0$, (25) and so as (11) cannot be satisfied and there are no complex k solutions, implying no power transfer.

Considering the reactive power terms, we can expand $\mathbf{V}^T\underline{\mathbf{Y}}_i^*\mathbf{V}^* + \mathbf{V}^T\underline{\mathbf{Y}}_{b,i}^*\mathbf{V}^* = 0$ as

$$\begin{aligned}&\frac{1}{\omega L'_{nn}}\sum_{n=1}^{N}\left(\beta^2-\omega^2L'_{nn}C'_{nn}\right)\left|\mathbf{t}_{I,n}^T\mathbf{V}\right|^2\\ &+\left(\beta^2(\beta_0-\beta)^2-3\alpha^2\beta_0^2+2\alpha^2\beta\beta_0\right)\lambda_1\,G_0\left|\mathbf{q}'^T_1\mathbf{V}\right|^2 = 0\end{aligned} \tag{26}$$

where $\mathbf{t}_{I,n}^T$ are the eigenvectors of $\underline{\mathbf{Y}}_i$ (that are also eigenvectors of $\underline{\mathbf{L}}^{-1}$) and $L'^{-1}_{nn}\left(\beta^2-\omega^2L'_{nn}C'_{nn}\right)$ are the eigenvalues of the real symmetric matrix $-\omega\underline{\mathbf{Y}}_i$. Once again, we observe that (26) is a sum of two contributions, the first from $\underline{\mathbf{Y}}_i$ and the second from $\underline{\mathbf{Y}}_{b,i}$, and we look for other conditions to find solutions assuming that $\beta > \beta_0$ (since there are none for $\beta < \beta_0$). It can be shown that the sign of the second term is always negative for $(\beta-\beta_0)^2 < \alpha^2$, which holds true in practical cases. Indeed, for example, in the one-TL case, one finds that $0 < \beta - \beta_0 = \beta_0 C_g/2 \ll \beta_0$ and $\alpha = \sqrt{3}\beta_0 C_g/2 > (\beta-\beta_0)$ [3]–[6]. Therefore, we find that the second term in (26) is always negative for $0 < \beta-\beta_0 < \alpha$. This means that if the resonance condition (11) is to be satisfied by a complex k, then the first term in (26) should have $\sum_{n=1}^{N}\left(\beta^2-\omega^2L'_{nn}C'_{nn}\right) > 0$. Recognizing that $\beta_{c,n}^2 = \omega^2L'_{nn}C'_{nn}$ [see discussion of (28) in Appendix B for definitions of notation], this means that $\beta \geq \max\left\{\beta_{c,1},\beta_{c,2},\ldots,\beta_{c,N}\right\}$, and $0 < \beta-\beta_0 < \alpha$ ensure that the resonance condition (26) can be always satisfied for any ω. If instead $\beta < \min\left\{\beta_{c,1},\beta_{c,2},\ldots,\beta_{c,N}\right\}$, then $\sum_{n=1}^{N}\left(\beta^2-\omega^2L'_{nn}C'_{nn}\right) < 0$ and the resonance condition (26), and hence (11), will not be satisfied. Therefore, we note

that a complex k solution is found when $0 < \beta - \beta_0 < \alpha$, and that the imaginary power $\mathrm{Im}S_S = (1/2)(\mathbf{V}^T \underline{\mathbf{Y}}^*_{b,i} \mathbf{V}^*)$ delivered *by* the beam (and delivered *to* the MTL) is positive.

To conclude, when $\beta > \beta_0$ and $\alpha > 0$, note that Y_b in Fig. 3 is capacitive since $\mathrm{Im}\,(Y_b) > 0$, and it has $\mathrm{Re}\,(Y_b) < 0$, hence it *delivers* positive time-average power to the whole circuit.

IV. Conclusion

We have presented an approach to extend the 1-D linearized Pierce model to multiple TLs coupled to a single electron beam. We have developed two formalisms to evaluate the k–ω dispersion relation including a matrix formulation and a formalism developed in terms of admittances. Both formalisms predict that the N-TL system coupled to electron beam has $2N+2$ solutions. Using the derived formalisms, we have predicted conditions that would always guarantee that the system supports growing waves. We have shown that if the electron propagation constant β_0 is greater than or equal to the largest of the circuit propagation constants $\beta_{c,n}$, then the system always supports a pair of increasing and decreasing waves in addition to N of forward and N backward waves. The condition is equivalent to stating that the electron velocity should be smaller than the smallest phase velocity among the N-TLs. In addition, we have shown that there exist other finite ranges of smaller electron propagation constant β_0 that also allow for a growing wave solution. These properties have also been verified numerically for some illustrative examples. On the TL side, the beam–line interaction was modeled as a distributed voltage-dependant shunt current source. It was found that for the growing wave solution, the beam always supplies power to the TLs. We anticipate that the theoretical framework developed in this paper could be used to design HPM devices incorporating multiple TLs with possible exploitation of DBEs in the Brillouin diagram when using periodicity along z.

Appendix A
Reduction of Determinant

The dispersion equation in (13) is derived from $\mathrm{Det}\left[\underline{\mathbf{M}} - k\underline{\mathbf{1}}\right] = 0$ by the use of determinant relation for partitioned matrices, $\mathrm{Det}\left[\begin{smallmatrix}\underline{\mathbf{A}} & \underline{\mathbf{B}} \\ \underline{\mathbf{C}} & \underline{\mathbf{D}}\end{smallmatrix}\right] = \mathrm{Det}\left(\underline{\mathbf{D}}\right) \mathrm{Det}\left(\underline{\mathbf{A}} - \underline{\mathbf{B}}\,\underline{\mathbf{D}}^{-1}\underline{\mathbf{C}}\right)$ [30], where, in general, the matrices $\underline{\mathbf{A}}$, $\underline{\mathbf{B}}$, $\underline{\mathbf{C}}$, and $\underline{\mathbf{D}}$ have sizes $M \times M$, $M \times L$, $L \times M$, and $L \times L$, respectively, and $\underline{\mathbf{D}}$ is an invertible matrix. In this particular case, the matrices are

$$\underline{\mathbf{A}} = \begin{bmatrix} -k\underline{\mathbf{1}} & \omega\underline{\mathbf{L}} \\ \omega\underline{\mathbf{C}} & -k\underline{\mathbf{1}} \end{bmatrix}$$

$$\underline{\mathbf{B}} = \begin{bmatrix} \mathbf{0} & \mathbf{0} \\ \omega\eta\frac{\rho_0}{u_0^2}\mathbf{s} & -\beta_0\mathbf{s} \end{bmatrix}$$

$$\underline{\mathbf{C}} = \begin{bmatrix} \mathbf{0} & -\omega\left(\mathbf{a}^T\underline{\mathbf{L}}\right) \\ \mathbf{0} & \mathbf{0} \end{bmatrix},$$

and

$$\underline{\mathbf{D}} = \begin{bmatrix} \beta_0 - k & 0 \\ -\omega\eta\frac{\rho_0}{u_0^2} & \beta_0 - k \end{bmatrix}.$$

Therefore, $\mathrm{Det}\left[\underline{\mathbf{M}} - k\underline{\mathbf{1}}\right] = 0$ can be expanded into the form

$$(\beta_0 - k)^2\,\mathrm{Det}\begin{bmatrix} -k\underline{\mathbf{1}} & \omega\underline{\mathbf{L}} \\ \omega\underline{\mathbf{C}} & -k\underline{\mathbf{1}} - \frac{k\omega^2\eta\rho_0}{u_0^2(k-\beta_0)^2}\mathbf{s}\mathbf{a}^T\underline{\mathbf{L}} \end{bmatrix} = 0. \quad (27)$$

In (27), we identify that each submatrix is of the same order $N \times N$. Therefore, using Schur's formulas [30] and after some algebraic manipulation, (27) is reduced to the final form of the dispersion equation in (13).

Appendix B
Growing Wave Condition

The matrices $\underline{\mathbf{L}}$, $\underline{\mathbf{C}}$ in (12) can be brought to a diagonal form $\underline{\mathbf{L}}'$, $\underline{\mathbf{C}}'$ using the modal decoupling technique subject to the conditions described in [27]–[29]. We transform (12) to the form (while following the notation in [27]–[29])

$$\mathrm{Det}\left(k^2\underline{\mathbf{1}} - \underline{\boldsymbol{\beta}_{\mathbf{c}}}'^2\right) \times\left[1+\frac{\eta\rho_0\beta_0^2k^2}{(k-\beta_0)^2}\left((\underline{\mathbf{T}}_V^T\mathbf{a})^T\left[\left(k^2\underline{\mathbf{1}}-\underline{\boldsymbol{\beta}_{\mathbf{c}}}'^2\right)^{-1}\underline{\mathbf{L}}'\right](\underline{\mathbf{T}}_V^T\mathbf{s})\right)\right] = 0 \quad (28)$$

where we define $\underline{\boldsymbol{\beta}_{\mathbf{c}}}'^2 = \omega^2\underline{\mathbf{T}}_V^{-1}\underline{\mathbf{L}}\,\underline{\mathbf{C}}\,\underline{\mathbf{T}}_{\mathrm{V}}$ and denote $\beta_{\mathbf{c},n}$ as the positive square root of the nth diagonal element of $\underline{\boldsymbol{\beta}_{\mathbf{c}}}'^2$. We note that $\mathrm{Det}(k^2\underline{\mathbf{1}} - \underline{\boldsymbol{\beta}_{\mathbf{c}}}'^2) = \prod_{n=1}^{N}(k^2-\beta_{\mathbf{c},n}^2)$ and $(k^2\underline{\mathbf{1}} - \underline{\boldsymbol{\beta}_{\mathbf{c}}}'^2)^{-1} = \sum_{n=1}^{N}(k^2-\beta_{c,n}^2)^{-1}$. When coupled to the electron beam, we assume $k = \beta_0 + \delta$ with $\delta \ll \beta_0$ and therefore $(k^2 - \beta_{c,n}^2) \approx 2\beta_0[\delta + \beta_{d,n}^2/(2\beta_0)]$, where we define $\beta_{d,n}^2 = \beta_0^2 - \beta_{c,n}^2$ and assume $|\beta_{d,n}^2| < \beta_0$ for $n = 1, 2, \ldots, N$. We assume $\mathbf{s} = \mathbf{a}$ and denote $\tilde{s}_n^2 = (\mathbf{t}_{V,n}^T\mathbf{s})^2 > 0$. We note that $\eta\rho_0 = I_0u_0/(2V_0)$, where V_0 is the dc beam voltage and $u_0^2 = 2\eta V_0$ [3] such that (28) can be simplified to the form

$$\delta^2\prod_{n=1}^{N}\left(\delta + \beta_{d,n}^2\,(2\beta_0)\right) + \sum_{m=1}^{N}\left[\tilde{s}_m^2\left(\omega L'_{mm}/(4V_0/I_0)\right)\prod_{\substack{n=1\\n\neq m}}^{N}\left(\delta + \beta_{d,n}^2/(2\beta_0)\right)\right] = 0$$

and is a sum of two terms. The first term is a polynomial in δ of degree $N+2$ with $N+1$ terms and the second term is a sum of N polynomials in δ, with each polynomial of degree $N-1$ and having $N-1$ terms with each polynomial containing the terms $\omega L'_{mm}\delta^n/(4V_0/I_0)$, which are ignored as they are very small since typically $4V_0/I_0$ is a very large number. On expanding and collecting common terms and substituting $M = N+2$, (28) can be written as a polynomial of degree $(N+2)$

$$P(\delta) = +\delta^M + c_{M-1}\delta^{M-1} + \cdots + c_3\delta^3 + c_2\delta^2 + c_0 = 0. \quad (29)$$

The coefficients $c_{M-1}, c_{M-2}, \ldots, c_0$ are formed from various combinations of $\beta_{d,n}^2/(2\beta_0)$ like, for example,

$$c_0 = \sum_{m=1}^{N}\left[\tilde{s}_m^2\left(\omega L'_{mm}/(4V_0/I_0)\right)\prod_{\substack{n=1\\n\neq m}}^{N}\left[\beta_{d,n}^2/(2\beta_0)\right]\right]$$

$$c_2 = \prod_{n=1}^{N}\left[\beta_{d,n}^2/\,(2\beta_0)\right] \text{ and } c_{M-1} = \sum_{n=1}^{N}\left[\beta_{d,n}^2/\,(2\beta_0)\right].$$

We find the following on the application of Descartes' rule of signs [33] to (29) and more information can be found in [34].

If $\beta_0 \geq \max\{\beta_{c,1}, \ldots, \beta_{c,N}\}$, it that implies all $\beta_{d,n} > 0$ and hence all coefficients $c_{M-1}, c_{M-2}, \ldots, c_0$ are purely real and positive. Hence, (29) has no positive roots, up to N negative roots (or decreased by multiple of two) and at least $(2, 4, \ldots, N, N+2)$ complex conjugate pairs of roots for any $\omega L'_{mm}/(4V_0/I_0) > 0$.

If $\beta_0 < \min\{\beta_{c,1}, \ldots, \beta_{c,N}\}$, it implies that all $\beta_{d,n} < 0$ and hence all coefficients $c_{M-1}, c_{M-2}, \ldots, c_0$ are real and negative. Hence, (29) has $N+1$ positive roots (or decreased by multiple of two), one negative root and at least $(2, 4, \ldots, N, N+1)$ complex conjugate pairs of roots for only certain values of $\omega L'_{mm}/(4V_0/I_0) > 0$. A rigorous proof in [32] states that (28) has at most two complex roots, and that these are always found if (18) is satisfied. The proof provided here using Descartes's rules only sets an upper bound to the number of real roots.

APPENDIX C
DATA FOR NUMERICAL EXAMPLES

The following are the parameters used to generate the plots in Figs. 5–8. The equivalent line inductances and capacitances for the helix were adapted from [15, Ch. 3]. However, these values are frequency dependent, and for simplicity, we assume certain indicative but physically realizable values of line inductances and capacitances. For the two-TL system whose real and imaginary parts of k are plotted in Fig. 5(a) and (b), we use $L_{11} = 1$, $L_{22} = 20$, $L_{12} = 0.1$ (all values in μH/m), $C_{11} = 200$, $C_{22} = 200$, $C_{12} = 10$ (all values in pF/m), and assume $\mathbf{s} = \mathbf{a} = \mathbf{1}$. Here, the nth TL has line inductance L_{nn} and line capacitance C_{nn} and the values of (L_{11}, C_{11}) and (L_{22}, C_{22}) are chosen such that they correspond to the inductance and capacitance values at the same frequency of two helices with different helix angles. The plots in Fig. 6 were generated using the same $\underline{\mathbf{L}}$ and $\underline{\mathbf{C}}$ matrix values used to generate the plots in Fig. 5. For the physical picture in Fig. 6(b), $\mathbf{s} = \mathbf{a} = \mathbf{1}$, for the physical picture in Fig. 6(c), $s_1 = a_1 = 1$ and $s_2 = a_2 = 0.1$, and for the physical picture in Fig. 6(d), $s_1 = a_1 = 0.1$ and $s_2 = a_2 = 1$. The plots in Fig. 7 were generated using $L_{11} = 10$, $L_{22} = 20$, $L_{12} = 0.1$ (all values in μH/m) and $C_{11} = 200$, $C_{22} = 200$, $C_{12} = 10$ (all values in pF/m). For the physical picture in Fig. 7(b), $\mathbf{s} = \mathbf{a} = \mathbf{1}$, for the physical picture in Fig. 7(c), $s_1 = a_1 = 1$ and $s_2 = a_2 = 0.1$, and for the physical picture in Fig. 7(d), $s_1 = a_1 = 0.1$ and $s_2 = a_2 = 1$. The parameters of the two-TL system with identical lines used to generate Fig. 8 are self-inductances and self-capacitances, which are given by $L_{11} = L_{22} = 10$ nH/m and $C_{11} = C_{22} = 10$ pF/m, respectively. The parameters of the one-TL system used for comparison in Fig. 6 are self-inductance and self-capacitance of the TL are $L = 1$ μH/m and $C = 200$ pF/m, respectively. For the physical picture in Fig. 8(a), $\mathbf{s} = \mathbf{a} = \mathbf{1}$, and for the physical picture in Fig. 8(b), $s_1 = a_1 = 1$ and $s_2 = a_2 = 0.1$ (also equivalent to $s_1 = a_1 = 0.1$ and $s_2 = a_2 = 1$ since both TLs are identical). In all the numerical calculations, the frequency of operation was assumed to be 1 GHz and the magnitude of line charge density is kept constant at $\rho_0 = 0.377$ nC/m.

ACKNOWLEDGMENT

The authors would like thanks to A. Figotin and G. Reyes from the Department of Mathematics, University of California, Irvine, CA, USA, for helpful discussions.

REFERENCES

[1] J. H. Booske and G. S. Nusinovich "Traveling-wave tubes (TWTs)," in *Modern Microwave and Millimeter-Wave Power Electronics*, R. J. Barker and N. C. Luhmann, Eds. Piscataway, NJ, USA: IEEE Press, 2005.
[2] J. R. Pierce and L. M. Field, "Traveling-wave tubes," *Proc. IRE*, vol. 35. pp. 108–111, Feb. 1947.
[3] J. R. Pierce, "Theory of the beam-type traveling-wave tube," *Proc. IRE*, vol. 35, no. 2, pp. 111–123, Feb. 1947.
[4] J. R. Pierce, "Waves in electron streams and circuits," *J. Bell Syst. Tech.*, vol. 30, no. 3, pp. 626–632, Jul. 1951.
[5] J. R. Pierce, *Traveling Wave Tubes*. Princeton, NJ, USA: Van Nostrand, 1950.
[6] A. S. Gilmour, *Principles of Traveling Wave Tubes*. Norwood, MA, USA: Artech House, 1994.
[7] J. R. Pierce, "Propagation in linear arrays of parallel wires," *IRE Trans. Electron Device*, vol. 2, no. 1, pp. 13–24, Jan. 1955.
[8] A. Karp, "Traveling-wave tube experiments at millimeter wavelengths with a new, easily built, space harmonic circuit," *Proc. IRE*, vol. 43, no. 1, pp. 41–46, Jan. 1955.
[9] E. A. Ash, "A new type of slow-wave structure for millimeter wavelengths," *Proc. IEE B, Radio Electron. Eng.*, vol. 105, no. 11, pp. 737–745, May 1958.
[10] E. A. Ash and A. C. Studd, "A ladder structure for millimeter waves," *IRE Trans. Electron Device*, vol. 8, no. 4, pp. 294–302, Jul. 1961.
[11] R. M. White, C. K. Birdsall, and R. W. Grow, "Multiple ladder circuits for millimeter wavelength traveling-wave tubes," in *Proc. Symp. Millim. Waves*, Apr. 1959, pp. 367–402.
[12] R. J. Barker and E. Schamiloglu, *High-Power Microwave Sources and Technologies*. New York, NY, USA: IEEE Press, 2005.
[13] J. S. Cook, R. Kompfner, and C. F. Quate, "Coupled helices," *J. Bell Syst. Tech.*, vol. 35, no. 1, pp. 127–178, Jan. 1956.
[14] G. Wade and N. Rynn, "Coupled helices for use in traveling-wave tubes," *IRE Trans. Electron Device*, vol. 2, no. 3, pp. 15–24, Jul. 1955.
[15] J. E. Rowe, *Nonlinear Electron-Wave Interaction Phenomena*. New York, NY, USA: Academic, 1965.
[16] J. L. Putz and G. C. Van Hoven, "Use of multiple helix circuits in 100-watt CW traveling-wave amplifiers," in *Proc. IRE Wescon Conv. Rec.*, Aug. 1957, pp. 138–142.
[17] C. K. Birdsall, "On the theory of traveling-wave tubes using paralleled electron streams," in *Proc. Symp. Millim. Waves*, Apr. 1959, pp. 341–355.
[18] A. Figotin and I. Vitebsky, "Gigantic transmission band edge resonance in periodic stacks of anisotropic layers," *Phys. Rev. E*, vol. 72, p. 036619, Sep. 2005.
[19] A. Figotin and I. Vitebsky, "Frozen light in photonic crystals with degenerate band edge," *Phys. Rev. E*, vol. 74, p. 066613, Dec. 2006.
[20] A. Figotin and I. Vitebsky, "Slow-wave resonance in periodic stacks of anisotropic layers," *Phys. Rev. A*, vol. 76, no. 5, p. 053839, Nov. 2007.
[21] A. Figotin and I. Vitebsky, "Slow wave phenomena in photonic crystals," *Laser Photon. Rev.*, vol. 5, no. 2, pp. 201–213, Mar. 2006.
[22] A. A. Chabanov, "Strongly resonant transmission of electromagnetic radiation in periodic anisotropic layered media," *Phys. Rev. A.*, vol. 77, p. 033811, Mar. 2008.
[23] C. Locker, K. Sertel, and J. L. Volakis, "Emulation of propagation in layered anisotropic media with equivalent coupled microstrip lines," *IEEE Microw. Wireless Compon. Lett.*, vol. 16, no. 12, pp. 642–644, Dec. 2006.
[24] G. Mumcu, K. Sertel, and J. L. Volakis, "Lumped circuit models for degenerate band edge and magnetic photonic crystals," *IEEE Microw. Wireless Compon. Lett.*, vol. 20, no. 1, pp. 4–6, Jan. 2010.
[25] S. Ramo, "Currents induced by electron motion," *Proc. IRE*, vol. 27, no. 9, pp. 584–585, Sep. 1939.
[26] W. Shockley, "Currents to conductors induced by a moving point charge," *J. App. Phys.*, vol. 9, no. 10, pp. 635–636, Oct. 1938.
[27] C. R. Paul, *Analysis of Multiconductor Transmission Lines*, 2nd ed. Hoboken, NJ, USA: Wiley, 2008.
[28] C. R. Paul, "Decoupling the multiconductor transmission line equations," *IEEE Trans. Microw. Theory Tech.*, vol. 44, no. 8, pp. 1429–1440, Aug. 1996.

[29] C. R. Paul, "A brief history of work in transmission lines for EMC applications," *IEEE Trans. Electromagn. Compat.*, vol. 49, no. 2, pp. 237–252, May 2007.
[30] D. S. Bernstein, *Matrix Mathematics: Theory, Facts and Formulas*, 2nd ed. Princeton, NJ, USA: Princeton Univ. Press, 2009.
[31] J. H. Booske and M. C. Converse, "Insights from one-dimensional linearized pierce theory about wideband traveling-wave tubes with high space charge," *IEEE Trans. Plasma Sci.*, vol. 32, no. 3, pp. 1066–1072, Jun. 2004.
[32] A. Figotin and G. Reyes. (Apr. 2013). *Multi-Transmission-Line-Beam Interactive System* [Online]. Avaliable: http://arxiv.org/abs/1304.5397
[33] X. Wang, "A simple proof of Descartes's rule of signs," *Amer. Math. Monthly*, vol. 111, no. 6, pp. 525–526, Jul. 2004.
[34] V. A. Tamma and F. Capolino. (Apr. 2013). *Extension of Pierce Model to Multiple Transmission Lines Interacting With an Electron Beam* [Online]. Avaliable: http://arxiv.org/abs/1304.5515

Venkata Ananth Tamma received the M.S. and Ph.D. degrees in electrical engineering from the University of Colorado, Boulder, CO, USA, in 2009 and 2012, respectively.

He has been a Post-Doctoral Fellow with the Department of Electrical Engineering and Computer Science, University of California, Irvine, CA, USA, since 2012. His current research interests include metamaterials, plasmonics, optical sensors, photovoltaics, and near-field optics.

Filippo Capolino (S'94–M'97–SM'04) received the Laurea (*cum laude*) and Ph.D. degrees in electrical engineering from the University of Florence, Florence, Italy, in 1993 and 1997, respectively.

He is currently an Associate Professor with the Department of Electrical Engineering and Computer Science, University of California, Irvine, CA, USA. He was an Assistant Professor with the Department of Information Engineering, University of Siena, Siena, Italy. From 1997 to 1999, he was a Post-Doctoral Fellow with the Department of Aerospace and Mechanical Engineering, Boston University, Boston, MA, USA. He was a Research Assistant Visiting Professor with the Department of Electrical and Computer Engineering, University of Houston, Houston, TX, USA, in 2000, 2001, and 2006. He was the EU Coordinator of the EU Doctoral Programs on Metamaterials from 2004 to 2009. His current research interests include antennas, metamaterials and their applications, sensors in both microwave and optical ranges, wireless systems, and chip-integrated antennas.

Dr. Capolino received the R. W. P. King Prize Paper Award from the IEEE Antennas and Propagation Society for the Best Paper of the Year in 2000. From 2002 to 2008, he served as an Associate Editor for the IEEE TRANSACTIONS ON ANTENNAS AND PROPAGATION. He is the Editor of the *Metamaterials Handbook* (Boca Raton, FL, USA: CRC Press, 2009).